Lattice-Boltzmann simulation of two-phase flow in porous media

C. Pan

Department of Environmental Sciences and Engineering, University of North Carolina, Chapel Hill, North Carolina, USA

M. Hilpert

Department of Geography and Environmental Engineering, Johns Hopkins University, Baltimore, Maryland, USA

C. T. Miller

Department of Environmental Sciences and Engineering, University of North Carolina, Chapel Hill, North Carolina, USA

Received 3 March 2003; revised 15 July 2003; accepted 21 August 2003; published 3 January 2004.

[1] We simulate two-fluid-phase flow at the pore scale using a lattice Boltzmann (LB) approach. Using a parallel processing version of the Shan-Chen model that we developed, we simulate a set of ideal two-fluid systems and a model two-fluid-phase porous medium system comprised of a synthetic packing with a relatively uniform distribution of spheres. We use the set of ideal two-phase systems to validate the approach and provide parameter information, which we then use to simulate a sphere-pack system. The sphere-pack system is designed to mimic laboratory experiments conducted to evaluate the hysteretic capillary pressure saturation relation for a system consisting of water, tetrachloroethylene, and a glass bead porous medium. Good agreement is achieved between the measured hysteretic capillary pressure saturation relations and the LB simulations when comparing entry pressure, displacement slopes, irreducible saturation, and residual entrapment. Our results further show that while qualitatively similar results are obtained when comparing systems consisting of 1200 spheres and 150 spheres, there is a significant difference between these two levels, suggesting a lower bound on the size of a representative elementary volume. *INDEX TERMS:* 1829 Hydrology: Groundwater hydrology; 1831 Hydrology: Groundwater quality; 1832 Hydrology: Groundwater transport; 1875 Hydrology: Unsaturated zone; *KEYWORDS:* lattice-Boltzmann, multiphase flow, two-phase

Citation: Pan, C., M. Hilpert, and C. T. Miller (2004), Lattice-Boltzmann simulation of two-phase flow in porous media, *Water Resour. Res.*, *40*, W01501, doi:10.1029/2003WR002120.

1. Introduction

[2] Multiple-fluid-phase (hereinafter simply multiphase) porous medium systems occur routinely in nature and are of significant interest within the water resources community. While the standard approach for modeling such systems relies upon a porous medium continuum scale representation [*Aziz and Settari*, 1979; *Abriola and Pinder*, 1985; *Abriola*, 1988; *Mayer and Miller*, 1990; *Miller et al.*, 1998], a significant body of work considers the more fundamental pore scale [*Lenormand and Zarcone*, 1988; *Cushman*, 1990; *Adler*, 1992; *Celia et al.*, 1995; *Lowry and Miller*, 1995; *Ferréol and Rothman*, 1995; *van Genabeek and Rothman*, 1996; *Pereira*, 1999; *Hilpert and Miller*, 2001]. While the majority of the pore-scale work has consisted of network models [e.g., *Koplik and Lasseter*, 1982; *Blunt and King*, 1991; *Oren and Pinczewski*, 1995; *Dillard and Blunt*, 2000; *Man and Jing*, 2000; *Blunt*, 2001; *Hilpert et al.*, 2001, 2003; *Thompson*, 2002], a growing interest is evolving in the use of lattice Boltzmann (LB) models for single [*Succi et al.*, 1989; *Martys et al.*, 1994; *Hou et al.*, 1995; *Bosl et al.*, 1998; *Maier et al.*, 1998; *D. Zhang et al.*, 2000; *Pan et al.*, 2001] and multiphase flow [*Rothman and Keller*, 1988; *Shan and Chen*, 1994; *Paunov et al.*, 1996; *Martys and Chen*, 1996; *Rothman and Zaleski*, 1997; *Chen and Doolen*, 1998; *Martys and Douglas*, 2001; *Hazi et al.*, 2002].

[3] LB models are growing in popularity because they provide a convenient means to simulate the true pore geometry of a porous medium system for both single-fluid and multiphase flow. Network models, by contrast, rely upon idealizations of the pore morphology and topology [*Blunt*, 2001]. We believe that the pore morphology and topology of real porous medium systems are extremely complex and that accurate pore-scale resolution of the porous medium will enable accurate and fruitful pore-scale simulations for a variety of fundamental purposes. However, while LB models have significant promise, they have received relatively little use in the water resources field. We believe that several reasons exist for the present situation: (1) LB modeling is a fairly recent method that is still evolving, so fewer codes have been developed for it than for traditional porous medium continuum and pore network modeling approaches [*van Genabeek and Rothman*, 1996; *Desplat et al.*, 2001; *Miller and Gray*, 2002]; (2) determining the pore structure of a porous medium is still extremely

0043-1397/04/2003WR002120$09.00

difficult in its own right and the subject of significant investigative research [*Lin and Cohen*, 1982; *Yao et al.*, 1993; *Soll et al.*, 1994; *Spanne et al.*, 1994; *Baldwin et al.*, 1996; *Sederman et al.*, 1997; *Mantle et al.*, 2001]; and (3) LB models are computationally very expensive—requiring efficient parallel implementations of the algorithms and access to large amounts of supercomputer time in order to simulate multiphase porous medium systems with sufficient resolution to provide meaningful results [*Kandhai et al.*, 1998; *Miller et al.*, 1998; *Hilpert and Miller*, 2001].

[4] These considerations notwithstanding, four general types of lattice Boltzmann models have been advanced to simulate multiphase flow systems. The first type is the so-called RK LB model for immiscible two-phase flow proposed by *Gunstensen et al.* [1991] and based on the original lattice gas model by *Rothman and Keller* [1988]. Gunstensen et al. used colored particles to distinguish between phases and applied a perturbation step so that Laplace's law is approximately recovered at an interface. The color model was further developed by later studies [*Grunau et al.*, 1993], but it has serious limitations. One of the most significant problems is that the model is not rigorously based upon thermodynamics, so it is difficult to incorporate microscopic physics into the model [*Boghosian and Coveney*, 2000; *He and Doolen*, 2002].

[5] The second type of LB approach (SC model) used to model multicomponent fluids was derived by *Shan and Chen* [1993, 1994] and later extended by others [*Shan and Doolen*, 1996; *Martys and Chen*, 1996; *Martys and Douglas*, 2001]. In the SC model, a nonlocal interaction force between particles at neighboring lattice sites is introduced. The net momentum, modified by interparticle forces, is not conserved by the collision operator at each local lattice node, yet the system's global momentum conservation is exactly satisfied when boundary effects are excluded [*Shan and Doolen*, 1996]. *Hou et al.* [1997] compared the above two types of models for simulating a static bubble in a two-fluid system and concluded that the SC model is a major improvement over the RK model. The main drawback of the SC model, however, is that it is not well-established thermodynamically. One can not introduce temperature since the existence of any energy-like quantity is not known [*He and Doolen*, 2002; *Hazi et al.*, 2002].

[6] The third type of LB model for multiphase flow is based on the free-energy (FE) approach, developed by *Swift et al.* [1995, 1996], who imposed an additional constraint on the equilibrium distribution functions. The FE model conserves mass and momentum locally and globally, and it is formulated to account for equilibrium thermodynamics of nonideal fluids, allowing for the introduction of well-defined temperature and thermodynamics [*Nourgaliev et al.*, 2003]. The major drawback of the FE approach is the unphysical non-Galilean invariance for the viscous terms in the macroscopic Navier-Stokes equation. Efforts have been made to restore the Galilean invariance to second-order accuracy by incorporating the density gradient terms into the pressure tensor [e.g., *Holdych et al.*, 1998; *Kalarakis et al.*, 2002, 2003].

[7] The fourth type of LB model has evolved from efforts to derive a thermodynamically consistent multiphase theory based upon the continuous Boltzmann equation [e.g., *Luo*, 1998; *He et al.*, 1998, 1999; *Ihle and Kroll*, 2000; *R. Zhang et al.*, 2000; *He and Doolen*, 2002; *Luo and Girimaji*, 2003]. This new class of model overcomes the unphysical features involved in the previous three types of multiphase LB models. While the preliminary work performed on this new class of model is encouraging, this type of model is still in active development, and it has not yet been extended to porous medium systems.

[8] The first three types of LB models have been employed increasingly for multiphase porous medium systems: to simulate the displacement of immiscible droplets in a channel [*Kang et al.*, 2002]; to study dispersion in two-phase flow through reconstructed porous media [*Bekri and Adler*, 2002]; to investigate relative permeability [*Martys and Chen*, 1996]; to study the contact line in a capillary tube [*Fan et al.*, 2001]; to model residual fluid entrapment [*Buckles et al.*, 1994; *Ferréol and Rothman*, 1995]; and to study contact angle hysteresis in capillary tubes [*Hazlett and Vaidya*, 2002]. However, most of these works were based either on two-dimensional models with simple geometries, or lacked quantitative comparison with experimental studies. Very few studies [*Martys and Chen*, 1996; *Yang et al.*, 2000; *Tolke et al.*, 2002; *Bekri et al.*, 2003] have reported simulations of multiphase flow in three-dimensional porous medium systems, in part because of the computational limitations noted above. To the best of our knowledge, no detailed comparisons between LB simulations and laboratory experiments for capillary pressure-fluid saturation relations have been reported in the peer-reviewed literature for three-dimensional multiphase systems.

[9] The specific objectives of this work are (1) to develop an efficient, parallel LB code capable of simulating two-fluid-phase flow in porous medium systems; (2) to validate our code by simulating a range of simple two-fluid systems; (3) to use simulation results from simple systems to guide parameter identification for more complex systems; (4) to investigate the discretization level necessary to achieve essentially resolution-independent results for two-fluid-phase flow in porous media; (5) to explore the domain size needed to obtain a representative elementary volume; and (6) to compare LB simulations with well resolved experimental measurements of hysteretic capillary pressure saturation relationships in two-fluid phase porous medium systems.

2. Simulation Model

2.1. Model Description

[10] We implemented the SC LB model [*Shan and Chen*, 1993, 1994] in three dimensions for a two-fluid-phase porous medium system, which is considered isothermal. The SC model allows for fluid phases with different wettabilities, densities, and viscosities. This model advances particle probabilities in time on a regular three-dimensional lattice, corresponding to 15 fixed velocity vectors per fluid phase, or component, using both an advection and a collision operator. The distribution function values, corresponding to probabilities, and model constants can in turn be used to deduce fluid densities and velocities. These results, together with model parameters, then help us discover fluid viscosities, the overall fluid velocity, pressure, and the contact angle between a wetting phase in contact with both the solid phase and the nonwetting fluid.

[11] The LB equation for the kth fluid is given by [*Shan and Chen*, 1993]:

$$f_i^k(\mathbf{x}+\mathbf{e}_i, t+1) - f_i^k(\mathbf{x}, t) = \frac{1}{\tau^k}\left[f_i^{k(eq)}(\mathbf{x}, t) - f_i^k(\mathbf{x}, t)\right], \quad i = 0, 1, \ldots, 14 \tag{1}$$

where $f_i^k(\mathbf{x},t)$ is the distribution function of the kth fluid component, which specifies the number of fluid particles of the species k at lattice location $\mathbf{x}$ and time t traveling in the ith direction; $\mathbf{e}_i$ is a lattice velocity vector that corresponds to allowable directions of the velocity vector; τ^k is the relaxation time of the kth fluid. The right-hand side of equation (1) represents the collision term, which is simplified to the equilibrium distribution function $f_i^{k(eq)}$ by the so-called BGK (Bhatnagar-Gross-Krook), or the single-time relaxation approximation [*Bhatnagar et al.*, 1954].

[12] The set of velocity vectors are defined as

$$\mathbf{e}_i = \begin{cases} (0,0,0), & i = 0 \\ \left(\delta_{1,i} - \delta_{2,i},\ \delta_{3,i} - \delta_{4,i}, \delta_{5,i} - \delta_{6,i}\right), & i = 1, \ldots, 6 \\ \left(1 - 2\left(\delta_{8,i} + \delta_{10,i} + \delta_{12,i} + \delta_{14,i}\right)\right., & \\ 1 - 2\left(\delta_{8,i} + \delta_{10,i} + \delta_{11,i} + \delta_{13,i}\right), & \\ \left.1 - 2\left(\delta_{8,i} + \delta_{9,i} + \delta_{12,i} + \delta_{13,i}\right)\right), & i = 7, \ldots, 14 \end{cases} \tag{2}$$

where $\delta_{j,i}$ is the Kronecker delta function. Equation (2) implies $|\vec{\mathbf{e}}_0| = 0$, $|\mathbf{e}_i| = 1$ for $i = 1, \ldots, 6$, and $|\mathbf{e}_i| = \sqrt{3}$ for $i = 7, \ldots, 14$.

[13] The macroscopic fluid density ρ^k, fluid velocity $\mathbf{v}^k$ and common velocity $\mathbf{v}$ are obtained by

$$\begin{aligned} \rho^k(\mathbf{x}, t) &= \textstyle\sum_i f_i^k(\mathbf{x}, t), \\ \mathbf{v}^k(\mathbf{x}, t) &= \textstyle\sum_i f_i^k(\mathbf{x}, t)\mathbf{e}_i / \rho^k(\mathbf{x}, t), \\ \mathbf{v}(\mathbf{x}, t) &= \textstyle\sum_k \left(\rho^k \mathbf{v}^k / \tau^k\right) \Big/ \sum_k \left(\rho^k / \tau^k\right). \end{aligned} \tag{3}$$

[14] The functional form of the equilibrium distribution $f_i^{k(eq)} = f(\rho^k, \mathbf{v}^{k(eq)})$ has the following form for the purpose of recovering the Navier-Stokes equation for each fluid component [*Chen et al.*, 1992; *Hou et al.*, 1997]:

$$f_i^{k(eq)} = \begin{cases} \dfrac{\rho^k \lambda^k}{7+\lambda^k} - \dfrac{1}{3}\rho^k \mathbf{v}^{k(eq)} \cdot \mathbf{v}^{k(eq)}, & i = 0 \\ w_i\left(\dfrac{\rho^k}{7+\lambda^k} + \dfrac{1}{3}\rho^k\left(\mathbf{e}_i \cdot \mathbf{v}^{k(eq)}\right) + \dfrac{1}{2}\rho^k\left(\mathbf{e}_i \cdot \mathbf{v}^{k(eq)}\right)^2 - \dfrac{1}{6}\rho^k \mathbf{v}^{k(eq)} \cdot \mathbf{v}^{k(eq)}\right), & i = 1, \ldots, 14 \end{cases} \tag{4}$$

where $w_i = 1$ for $i = 1, \ldots, 6$, and $w_i = 1/8$ for $i = 7, \ldots, 14$. λ^k in equation (4) is an adjustable parameter that can be chosen in the admissible range limited by numerical stability.

[15] When the above equilibrium distribution function is chosen, the pressure of a pure kth fluid component P^k is given by [*Shan and Chen*, 1993; *Hou et al.*, 1997]

$$P^k = \left(C_s^k\right)^2 \rho^k = \frac{3}{7+\lambda^k}\rho^k. \tag{5}$$

In equations (4) and (5), λ^k is a parameter that is related to the speed of sound C_s^k. The corresponding kinematic viscosity ν^k is $(2\tau^k - 1)/6$. With the long-range interparticle forces included in the model, besides the momentum change of the kth fluid due to the collisions with other fluids, there exists an extra momentum change due to interaction forces. Hence the equilibrium velocity $\mathbf{v}^{k(eq)}$ in equation (4) is defined as [*Shan and Chen*, 1993, 1994]

$$\rho^k \mathbf{v}^{k(eq)} = \rho^k \mathbf{v} + \tau^k \mathbf{F}^k, \tag{6}$$

where $\mathbf{F}^k$ is the total interaction force on the kth fluid component, including the fluid-fluid and fluid-solid interactions.

2.2. Fluid-Fluid Interaction Force

[16] In the SC model, nearest-neighbor interactions are used to define the interparticle forces. $\mathbf{F}_{f-f}^k(\mathbf{x})$, the fluid-fluid interaction force on kth fluid at site $\mathbf{x}$ is the sum of the forces between the kth fluid particle at $\mathbf{x}$ and the k'th fluid particles at neighboring sites $\mathbf{x}'$

$$\mathbf{F}_{f-f}^k(\mathbf{x}) = -\psi^k(\mathbf{x}) \sum_{\mathbf{x}'} G_{kk'}(\mathbf{x}, \mathbf{x}')\psi^{k'}(\mathbf{x}')(\mathbf{x}' - \mathbf{x}), \tag{7}$$

where $\psi^k(\rho^k)$, the so-called "effective mass" [*Shan and Doolen*, 1995], is a function of local density and $G_{kk'}$ represents the strength of the interpartical force. In our study $\psi^k = \rho^k$ is used for simplicity; other choices of ψ^k lead to different equations of state for the composite fluid [*Shan and Chen*, 1994; *Shan and Doolen*, 1995]. In equation (7), $G_{kk'} = G_{k'k}$ is a symmetric matrix based upon a Green's function of the form

$$G_{kk'}(\mathbf{x}, \mathbf{x}') = \begin{cases} g & \text{if} \quad |\mathbf{x} - \mathbf{x}'| = 1 \\ g/\sqrt{3} & \text{if} \quad |\mathbf{x} - \mathbf{x}'| = \sqrt{3} \\ 0 & \text{otherwise,} \end{cases} \tag{8}$$

where g is the fluid-fluid interaction coefficient. By choosing the sign and the magnitude of g properly, fluids can separate so that immiscible flow behavior motivated by interfacial tension can be simulated [*Hou et al.*, 1997].

2.3. Fluid-Solid Interaction Force

[17] The interaction force between the kth fluid at site $\mathbf{x}$ and the solid wall at site $\mathbf{x}'$ is formulated as [*Martys and Chen*, 1996]:

$$\mathbf{F}_{f-s}^k(\mathbf{x}) = -\rho^k(\mathbf{x}) \sum_{\mathbf{x}'} G_{ks}(\mathbf{x}, \mathbf{x}')s(\mathbf{x}' - \mathbf{x}). \tag{9}$$

At the fluid-solid interface, the solid is regarded as a phase with constant density s, which is 1 for a solid and 0 for a pore. To be consistent with the fluid-fluid interaction coefficient, we let

$$G_{ks}(\mathbf{x}, \mathbf{x}') = \begin{cases} g_{ks} & \text{if} \quad |\mathbf{x} - \mathbf{x}'| = 1 \\ g_{ks}/\sqrt{3} & \text{if} \quad |\mathbf{x} - \mathbf{x}'| = \sqrt{3} \\ 0 & \text{otherwise,} \end{cases} \tag{10}$$

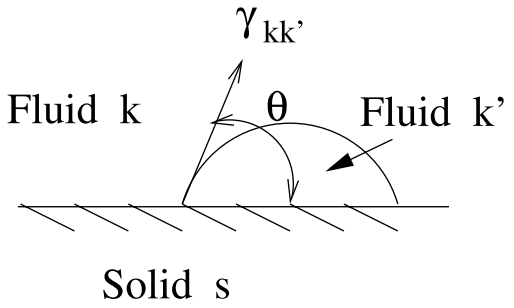

Figure 1. Contact angle between a fluid-fluid interface and a solid wall. Here γ represents the interfacial tension between fluids, and θ denotes the contact angle.

where g_{ks} represents the interactive strength between the kth fluid and the solid phase. One can choose the sign and the magnitude of g_{ks} to distinguish the different wetting properties of pure fluids. The sign of g_{ks} shows whether component k is attractive (negative sign) or repulsive (positive) to the solid phase. By adjusting the g_{ks} for each fluid, a desired contact angle θ between a fluid-fluid interface and a solid, as illustrated in Figure 1, can be obtained.

[18] With the presence of interparticle forces $\mathbf{F}^k = \mathbf{F}^k_{f-f} + \mathbf{F}^k_{f-s}$, the collision operator does not conserve momentum locally, as shown in equation (6). Nevertheless, since $G_{kk'}$ defined in equation (8) is a symmetric matrix, the momentum of the whole fluid system is conserved, provided that only fluid-fluid interactions are considered and that there is no net momentum flux from the boundary conditions [*Shan and Doolen*, 1995]. We ignore the external body force in the model because the systems of concern in this work are dominated by capillary forces.

[19] The continuity and momentum conservation equations for the whole fluid can be obtained by the Chapman-Enskog expansion [*Shan and Chen*, 1993; *Shan and Doolen*, 1995]. With the above definition of the fluid-fluid interaction force and the lattice structure, we can derive the following equation of state in a straightforward manner:

$$P = \left[\sum_k \left(C_s^k\right)^2 \rho^k\right]\mathbf{I} + \left(2 + \frac{8}{\sqrt{3}}\right)\sum_k\left(1 - \frac{1}{2\tau^k}\right)\sum_{k'} g\psi^k\psi^{k'}, \tag{11}$$

where P is the overall fluid pressure. The second term on the right-hand side of equation (11), which represents a nonideal gas law, depends explicitly on the fluid-fluid interaction force $\mathbf{F}^k_{f-f}$. Note that the fluid-solid interaction force $\mathbf{F}^k_{f-s}$ exists only on the fluid-solid interface, so it does not affect the macroscopic fluid equations [*Kang et al.*, 2002]. The overall fluid velocity $\mathbf{u}$ is defined as $\rho\mathbf{u} = \Sigma_k\Sigma_i f_i^k\mathbf{e}_i + \frac{1}{2}\Sigma_k\mathbf{F}^k$ [*Shan and Doolen*, 1995], where $\rho = \Sigma_k\rho^k$ is the total density of the fluids.

3. Experimental System

[20] A primary goal of this work is to compare two-fluid-phase LB simulations with experimental measurements of a hysteretic capillary pressure-saturation ($P - S$) relation; we summarize briefly a series of NAPL-water displacement experiments reported by Hilpert et al. (2001), which we used for this purpose. A 1-m long × 2.5 cm-diameter porous medium column was used to examine the capillary $P - S$ relation in a glass bead packing, labeled as GB1b. Dyed tetrachloroethylene (PCE) and water were the nonwetting phase (NWP) and wetting phase (WP), respectively. The bottom and the top of the column were connected to a constant pressure NWP and WP reservoirs, respectively. Various vertical equilibrium saturation profiles were obtained by successive changes of the reservoir elevations. Provided that the porous medium is homogeneous throughout the long vertical column, the column approach is analogous to a retention-cell experimental procedure with no gravity effect [*Schiegg*, 1979, 1990] in which the $P - S$ relation is measured by using step changes in the elevation of the constant-head fluid reservoirs. Table 1 summarizes the properties of the experimental GB1b system.

[21] Constitutive relations for multiphase flow in porous media are dominated by capillary forces at the pore scale. Gravity and viscous forces also contribute to multiphase flow behavior. To evaluate the effect of these forces for the experimental system considered, three nondimensional variables, the capillary number Ca, which describes the ratio of viscous forces to capillary forces, the viscosity ratio M, and the Bond number Bo, which describes the ratio of gravity forces to capillary forces, are often used and defined as [*Mayer and Miller*, 1992]:

$$Ca = v_w\mu_w/\gamma$$
$$M = \mu_n/\mu_w \tag{12}$$
$$Bo = g_c(\rho_n - \rho_w)R^2/\gamma$$

where v_w is the aqueous phase Darcy velocity, g_c is the gravitational constant, and R is the mean pore radius. The values of M and Bo are listed in Table 1. Viscous forces were insignificant because of the quasi-static nature of the experiments and the small incremental steps taken in the redistribution process.

4. Model Calibration

[22] The primary physical parameters that must be determined in the two-phase LB model include densities and viscosities of fluids, as well as the fluid-fluid and fluid-solid interaction coefficients. To calibrate these nondimensional model parameters, two types of numerical experiments were conducted: bubble tests in the absence

Table 1. Properties of the Experimental GB1b Multiphase System

Property	Value
Arithmetic diameter $\overline{D}$ (mm)	0.1156 ± 0.0121
Porosity ϕ	0.356 ± 0.002
NWP and WP	dyed PCE and water
NWP density ρ_n (g/cm^3)	1.613 ± 0.002
WP density ρ_w (g/cm^3)	0.998 ± 0.002
NWP viscosity μ_n (cp)	1.844
WP viscosity μ_w (cp)	1.0
Interfacial tension γ (dyn/cm)	36.23 ± 0.21
Viscosity ratio M	1.844
Bond number Bo	8.9×10^{-5}

of a solid phase and displacement tests of one fluid by the other in axially symmetric tubes.

4.1. Bubble Test

[23] Test problems were simulated for both two-dimensional and three-dimensional bubbles. The domain size in the two-dimensional bubble test was 64 × 64 × 3 lattice units, with a cylindrical NWP bubble with a circular cross section in the *xy* plane located in the middle of the domain. For the three-dimensional bubble test, the domain size was 64 × 64 × 64 lattice units with a spherical NWP bubble inside. Periodic boundary conditions were used in all three directions. Initially, a NWP bubble with a certain radius was immersed totally in the WP. At steady state, in the absence of a solid phase and body forces, each fluid phase has a constant pressure at the interface. The pressure difference P^c across the fluid interface is related to the radius R of the steady state NWP bubble by Laplace's law [*Bear*, 1972]:

$$P_n - P_w = P^c = c\frac{\gamma}{R} \quad (c = 1 \text{ for 2-D}, \quad c = 2 \text{ for 3-D}) \quad (13)$$

[24] The model parameters needed for the bubble test were initial densities ρ_n and ρ_w both inside and outside the bubble, relaxation times τ_n and τ_w, equilibrium distribution parameters λ_n and λ_w, and the fluid-fluid interaction coefficient g. To distinguish between nondimensional model variables and the physical quantities, the latter are marked with a superscript *. Common dimensional equations are: $v^* = v_0 v$, $\rho^* = \rho_0 \rho$, $P^* = \rho_0 v_0^2 P$, $R^* = l_0 R$ and $v^* = v_0 l_0 v = v_0 l_0 (2\tau - 1)/6$, where variables with a subscript 0 are the characteristic variables used to represent a physical system.

[25] We matched the dynamic viscosity ratio M between fluids, which is an important parameter for fluids displacement [*Dias and Payatakes*, 1986]:

$$M = \frac{\mu_n^*}{\mu_w^*} = \frac{\nu_n^* \rho_n^*}{\nu_w^* \rho_w^*} = \frac{(2\tau_n - 1)\rho_n}{(2\tau_w - 1)\rho_w} \quad (14)$$

There are two ways to achieve the desired dynamic viscosity ratio: one is to match both the density ratio and kinematic viscosity ratio (for simplicity, we call it case 1); the other is to assume the same nondimensional density for both fluids and match the dynamic viscosity ratio desired by adjusting the kinematic viscosity of the two fluids (case 2), which is a reasonable approach if body forces are neglected, as they are in this work because of capillary force dominance.

[26] For case 1, in which both ratios match real values, we chose $\tau_n = 1$, so τ_w was computed as 0.94 according to equation (14). We further let $\rho_n = 150$, hence ρ_w was 93. According to equation (11), we chose λ_n and λ_w from the following, in order to have equal pressures for the pure fluid phases:

$$\frac{3}{7 + \lambda_n}\rho_n = \frac{3}{7 + \lambda_w}\rho_w. \quad (15)$$

Realizing that λ cannot be arbitrarily chosen because of its effect on numerical stability for this model, we let $\lambda_w = 1$, so $\lambda_n = 5.9$.

[27] For case 2, in which the density ratio was not matched, we let $\rho_n = \rho_w = 150$ and $\lambda_n = \lambda_w = 2$, the same λ value used in our previous single-phase LB model [*Pan et al.*, 2001]. We also chose $\tau_w = 1$ and $\tau_n = 1.42$ to match M.

[28] The initial fluid densities in case 1 were $\rho_n = 150$ and $\rho_w = 0$ inside the bubble, and $\rho_n = 0$ and $\rho_w = 93$ outside. In case 2, similar values were used other than $\rho_w = 150$ outside the bubble. Those initial densities differed from that of *Hou et al.* [1997], who claimed that there must be a small amount of WP fluid inside the bubble and a small amount of NWP fluid outside the bubble for numerical stability. We did not experience the instability problem with initially zero NWP and WP densities outside and inside the bubble, respectively. Compared to Hou et al.'s setting, we observed slightly larger fluctuations of fluid densities during the first ten iterations, after which the fluctuation decreased to a negligible level. Steady state was considered to be achieved when the following criterion was satisfied:

$$\frac{\sqrt{\sum_{\mathbf{x}} [\mathbf{u}(\mathbf{x}, t) - \mathbf{u}(\mathbf{x}, t - 50)]^2}}{\sqrt{\sum_{\mathbf{x}} \mathbf{u}(\mathbf{x}, t)^2}} < 10^{-6}. \quad (16)$$

[29] In simulations of both cases, the fluid interaction coefficient g was set to 0.001. If g was less than 0.001, the interaction force between fluids was not large enough to produce the desired phase separation, while a larger g value ($g > 0.0012$) led to larger spurious velocities at the fluid-fluid interface, and consequently negative distribution functions, and numerical instability. Negative distribution functions were more likely to occur for case 1 where a larger value of λ was used ($\lambda_n = 5.9$) than for case 2.

[30] At steady state, the fluid pressures across the interface were determined by equation (11). To test Laplace's law, shown in equation (13), we carried out simulations with various initial bubble radii. Radius R of the steady state bubble was calculated as described by *Hou et al.* [1997]. The pressure differences across the interface are plotted with respect to R in Figure 2, which shows good agreement with Laplace's law for both cases. The slope of the linear fit is the nondimensional interfacial tension γ, which was determined as 14.68 for case 1 and 22.71 for case 2.

[31] Although both cases with different parameter settings agree well with Laplace's law, we chose to follow the case 2 approach for all subsequent work reported herein. We based this choice upon the physical equivalence of the two methods for the systems of concern and the more stable nature of the simulations under case 2 conditions.

4.2. Two-Fluid Displacement Test in Capillary Tubes

[32] With the presence of the solid phase, two more important parameters, namely nonwetting-solid and wetting-solid interaction coefficients g_{ns} and g_{ws}, should be determined to ensure the desired static contact angle. Because the experimental system was assumed to be totally water-wet, the contact angle θ was set to zero. To ensure this condition was met, we carried out fluid displacement simulations on simple capillary tubes for which the physical behavior is known analytically and depends upon the contact angle.

4.2.1. Setup of Displacement Simulation

[33] Figure 3 illustrates our simulation approach that aims to mimic the quasi-static experimental displacement experiments performed and described in section 3. We added NWP and WP reservoirs, consisting of two additional layers

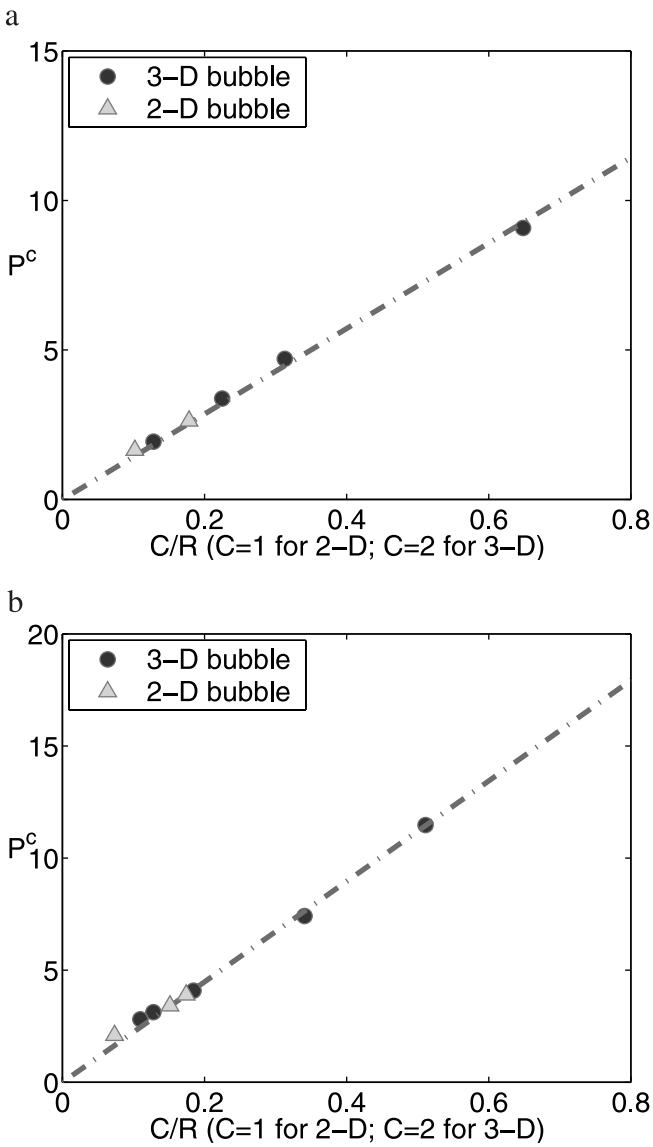

Figure 2. Test of Laplace's law: (a) case 1 and (b) case 2.

of void space, at both horizontal ends of the simulated system. In addition, to be consistent with the experimental setup, we simulated a water-wet porous plate with a checkboard lattice comprised of alternating voxels of solid and void space, which is illustrated in Figure 3.

[34] The boundary conditions of the three-dimensional simulations were periodic except for the horizontal x direction. Fixed pressure boundary conditions (equivalent to fixed densities) were applied to the first layer of the NWP reservoir and to the last layer of the WP reservoir. The fixed density boundary conditions were implemented by updating the distribution functions after each collision step with the equilibrium distribution functions that have zero velocity and the desired densities. Because the curved boundaries of the solid phase in the porous media were digitized into a regular lattice using a zigzag staircase approach, the boundary conditions at fluid-solid interfaces were applied directly by the bounce-back scheme for the no-slip boundary condition by reflecting fluid particles moving toward a solid boundary back toward the fluid node from which they originated. This approach is second-order accurate, but does introduce a discretization error for the spherical solid phase particles of interest in this work. Lattice refinement studies were used to ensure convergence of this approximate discrete approach.

[35] To simulate the primary drainage (PD) process, we started from zero capillary pressure, which was achieved by fixing NWP and WP densities in the first layer of the NWP reservoir to be 150 and 0, respectively, and 0 and 150 in the last layer of the WP reservoir, respectively. Then the capillary pressure P^c was increased incrementally by decreasing the WP density in the WP reservoir and keeping all other fluid densities on the boundaries constant at their original values. This process resulted in stable, well-behaved numerical simulations. Driven by the pressure gradient, NWP entered the medium and displaced the WP in the initially WP-saturated porous medium. Imbibition processes were simulated by decreasing the P^c. Because the NWP density in the NWP reservoir did not change during the simulation, we considered a lattice node as being occupied by NWP when NWP density at this node was

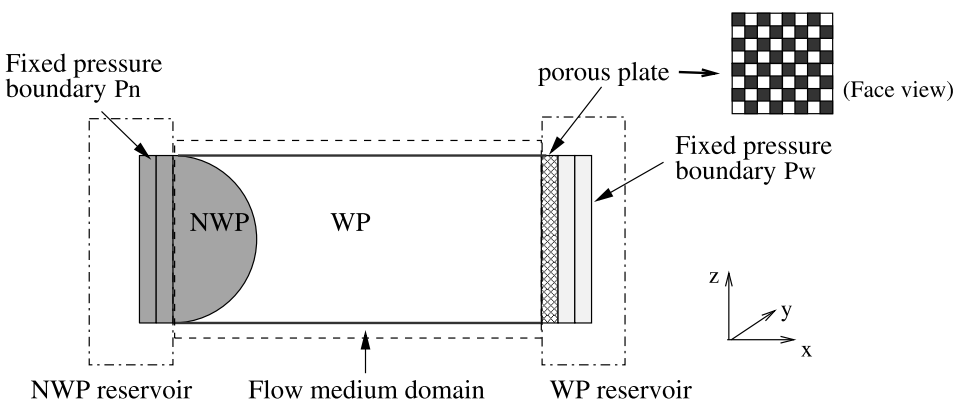

Figure 3. Setup of the two-fluid displacement simulation. The left side of the medium domain locates the nonwetting phase reservoir, and the right side locates the wetting phase reservoir. A porous plate is located between the flow domain and wetting phase reservoir, which serves as a capillary barrier to NWP exit. Black and white blocks in the porous plate stand for the solid and fluid spaces, respectively.

larger than half of the fixed NWP reservoir density, otherwise this node was assumed to be WP occupied. To mimic quasi-static displacement experiments, LB simulations proceeded solving at a discrete set of time steps until steady state was achieved after each adjustment in P^c. Steady state was determined when either equation (16) was satisfied, or the number of voxels occupied by each fluid remained unchanged after 400 time steps.

4.2.2. Test Results

4.2.2.1. Flow Through Capillary Tubes

[36] We designed three test problems for flow through cylindrical capillary tubes with cross sections of different shapes, for which the behavior of the fluid displacement can be calculated analytically. The first type of tube had a square-shaped pore geometry, and the length of the pores was 4, 8, and 16 lattice units for domain sizes 16^3, 32^3, and 64^3, respectively. The pore space in the second type of tube had a rectangular cross section. Again, we studied three resolution levels with domain sizes of 16^3, 32^3, and 64^3 lattice units, in which the length L_1 and width L_2 of the rectangular pore space were 12×6, 24×12, and 48×24 lattice units, respectively. It is known that the mean radius of curvature $R = 1/(2/L_1 + 2/L_2)$ for the case of zero contact angle [*Bear*, 1972]. The third type of capillary tube had a cross section shown in Figure 4, i.e., the pore space was formed by four grains of uniform radius. For this geometry, we generated three domains of 20^3, 40^3, and 60^3 voxels, with corresponding grain radii R_g being 5, 10, and 15 lattice units. We know that the inscribed radius of the pore space $R = \left(\sqrt{2} - 1\right)R_g$.

[37] On the basis of simulation results and numerical stability considerations, we chose $g_{ns} = -0.02$ and $g_{ws} = 0.02$ to ensure a zero contact angle. These parameter values differ from the results of *Fan et al.* [2001], who found that g_{ns} and g_{ws} have to be small compared with the fluid-fluid interaction parameter g. Figure 5 plots the nondimensional pressure $P^{c'} = P^cR/\gamma$ versus the wetting phase saturation S_w for the three capillary tubes, obtained from LB simulations. We obtained good agreement of the simulated and analytical NWP entry pressure, which is the minimum pressure

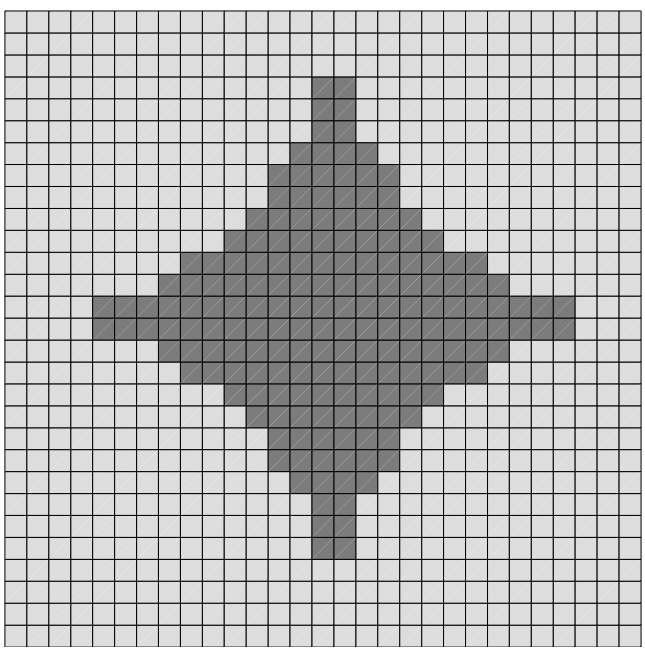

Figure 4. Cross section of the third type of capillary tube. The dark section in the middle is the pore space.

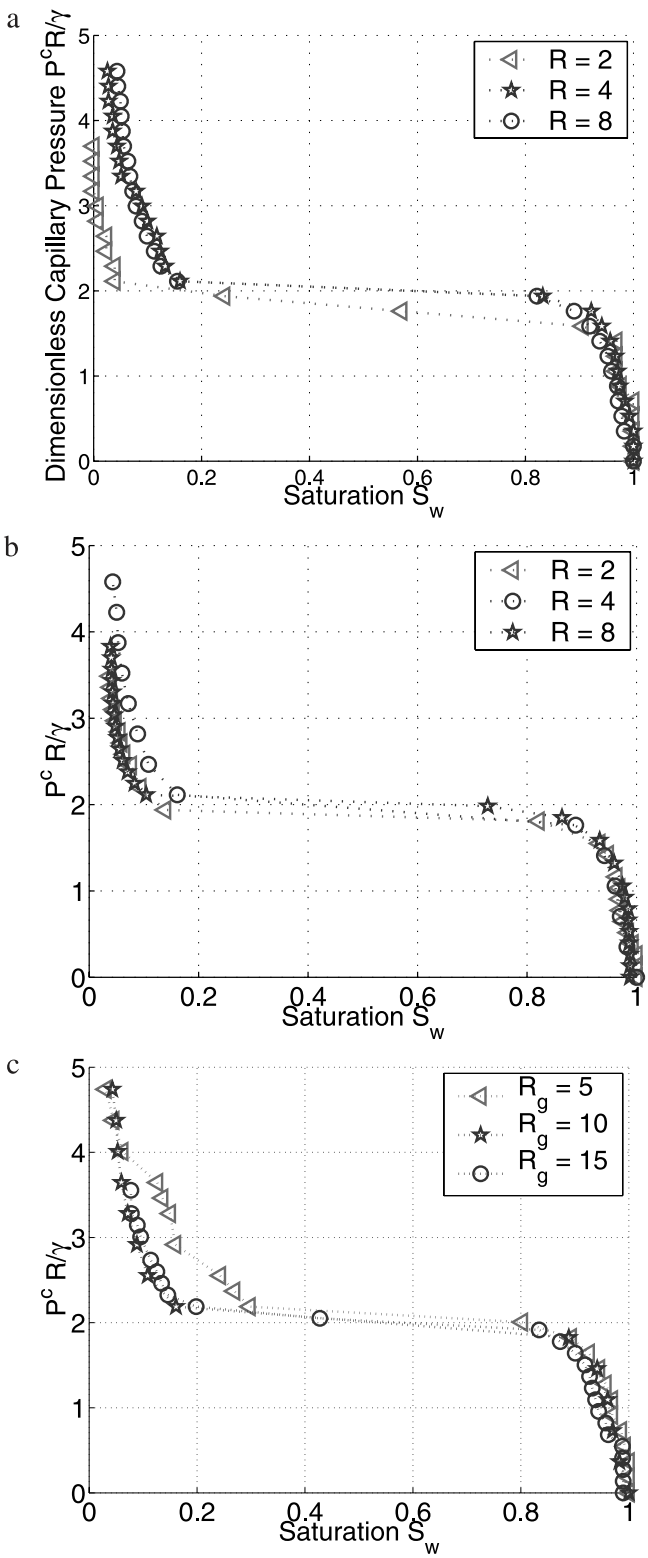

Figure 5. Primary drainage curves obtained by fluid displacement simulations in capillary tubes with cross sections of different shapes: (a) square-shaped cross section, (b) rectangular cross section, and (c) a pore space formed by the intersection of four uniform circles, as shown in Figure 4.

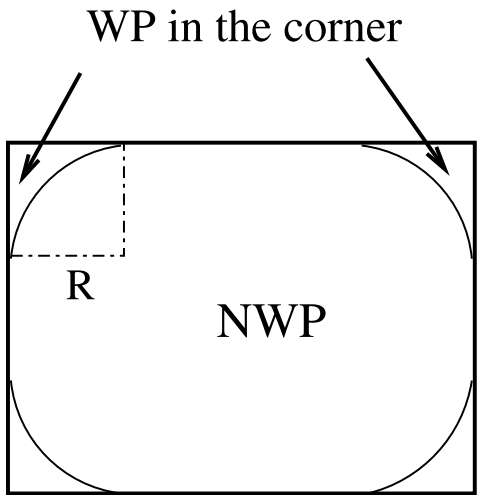

Figure 6. Amount of wetting phase in the corner of a rectangular pore space.

needed to initiate the WP displacement; the analytical entry pressure is 2.0 according to Laplace's law. We did not see a strong discretization effect on NWP entry in Figure 5a and 5b, because the digital representation of the square-shaped or rectangular pore space is exact. We did observe discretization effects on the shape of the PD curves for all three types of pore geometries; for increasing discretization levels, the shoulder of the PD curve at the entry point becomes shaper.

[38] We also obtained good agreement between the LB prediction and the analytical value for the amount of WP in the corner of the pore channel. As shown in Figure 6, the WP saturation S_w for a pore channel with rectangular cross section can be computed as:

$$S_w = f(P^c) = 4(1 - \pi/4)R^2/A_p \tag{17}$$

where A_p is the area of the pore cross section, and R is the radius of curvature corresponding to a P^c. For example, in a medium with a rectangular pore space consisting of a 24 × 12 lattice units, the WP saturation is computed analytically as 0.05 at P^c = 11.0, which corresponds to a radius of curvature R = 4.1, because γ = 22.71 from the previously reported bubble test. The LB simulation predicted the WP saturation also as 0.05, and, for a more finely resolved medium of 48 × 24 lattice units, a WP saturation of 0.04 was computed, as shown in Figure 5b (at P^cR/γ = 3.8).

4.2.2.2. Flow Through a Channel With Two Different Throat Diameters

[39] We then simulated the PD process in a medium with a more complicated pore geometry, containing two pore throats, whose radii were 6 and 4 lattice units, respectively. Figure 7 illustrates the medium geometry and the steady state NWP distribution patterns at different P^c. From the interfacial tension coefficient γ determined from the previous bubble test, we estimated entry pressures P^c for both throats as 7.5 and 11.25, respectively. These estimates are consistent with the simulation results shown in Figure 7.

[40] We monitored the behavior of *Ca* during the fluid displacement simulation. *Ca* was computed on the outlet porous plate layer, the pore space of which was entirely occupied by the wetting phase. In Figure 8 we show the time evolution of *Ca* during the simulation, including five step changes of P^c. Figure 8 shows clearly that *Ca* drops down to 10^{-5} to 10^{-6} when the simulation approached steady state at each capillary pressure step. However, *Ca* did not further approach zero, because in the SC LB model there always exists nonzero velocity in the interface region, which has been called a spurious current [*Hou et al.*, 1997]. *Ca* was computed to support the use of an adaptive pressure step change scheme to save computational time during fluid displacement simulations. Instead of using a uniform capillary pressure step change ΔP^c between quasi-static steps, we chose ΔP^c depending upon the *Ca* computed after quasi-static convergence at a given P^c by

$$\Delta P^{c,l+1} = \begin{cases} \Delta P^{c,l} & \text{if} \quad Ca > 10^{-6} \\ 2\Delta P^{c,l} & \text{otherwise.} \end{cases} \tag{18}$$

where l is an index for the set of P^c simulated. We found that we could save >20% of the computational time by using the above adaptive approach without significantly

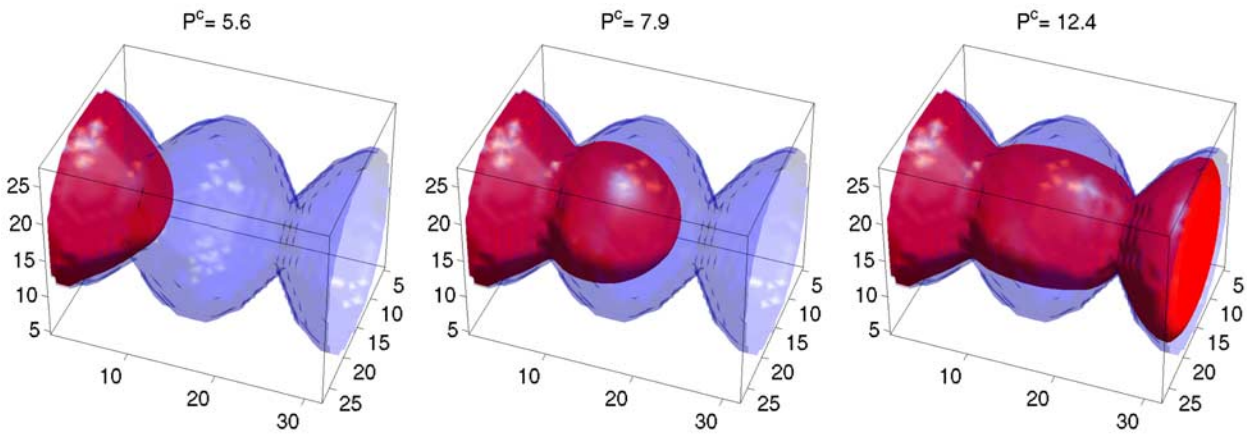

Figure 7. Patterns formed by a nonwetting phase displacing a wetting phase at different capillary pressures. The medium had pore throats with diameters 12 and 8 lattice units, respectively. The transparent blue isosurface represents the interface between the pore space and the solid phase. The

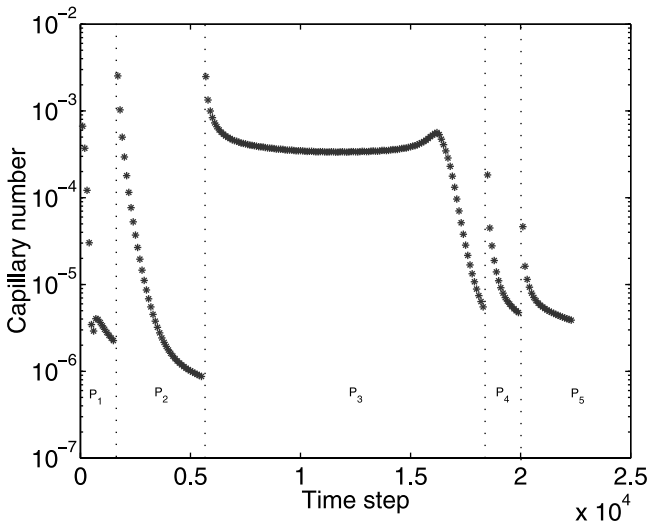

Figure 8. Time evolution of capillary number during a fluid displacement simulation with five step changes of capillary pressure.

changing our results. Thus we applied the approach in the following porous medium simulations.

5. Simulation of Two-Phase Flow Displacement in Porous Media

5.1. Two-Phase Flow Through an Idealized Sphere Packing Porous Media

[41] We used the above noted parameters to simulate two-fluid-phase flow through porous media. We emphasize that the set of the model parameters is not unique, the determination of which was based upon the analysis of results from the specific tests described above, considerations of simplicity, and numerical stability.

[42] As a validation step for our approach and our estimated parameter values, we first applied the LB model to an idealized porous medium. The medium consisted of 8 spheres of equal diameter, packed as shown in Figure 9. We discretized the medium with lattices of 20^3, 30^3, 40^3, and 80^3 units with sphere radii $R_g = 5$, 7.5, 10, and 20 lattice units, respectively. Primary drainage simulations were performed for all four discretization levels.

[43] Figure 10 shows the relationship between the capillary pressure, $P^{c'} = P^c R_g/\gamma$, as a function of WP saturation S_w. From Figure 10 we observed that at a discretization level $R_g = 7.5$, the LB simulation for the PD process approaches convergence. In addition, LB simulations predict that the NWP entry $P^{c'}$ is approximately 5, so one can estimate that $P^c R/\gamma$ is close to the analytical value of 2 because the pore throat radius R is given analytically by $R = (\sqrt{2} - 1)R_g$.

5.2. Two-Phase Flow Through a Simulated Porous Medium

[44] After validating the LB model for two-phase flow in simple channels and an ideal porous medium, we then performed simulations in a simulated porous medium, which was intended to be representative of the experimental GB1b medium described in section 3. The experimental GB1b medium was represented using a random sphere pack generated by *Hilpert and Miller* [2001] using the algorithm and

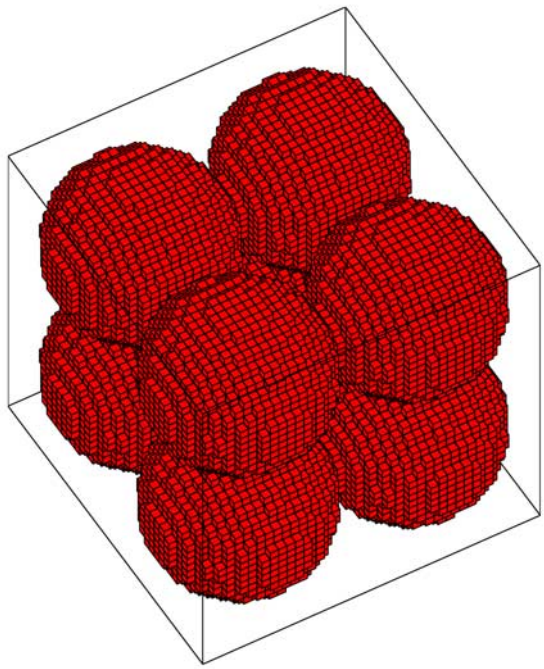

Figure 9. An idealized porous medium packed with eight spheres of equal diameters.

code developed by *Yang et al.* [1996]. Simulated porous media can be readily generated using this approach and matched to the porosity and probability density function measures of the grain size for a real porous medium. Of course, this is an idealized step since the real media were not perfect spheres and the packing generated only approximately matched the macroscopic measures of the experimental media and not the exact morphology and topology of the pore space in the experimental system. Good agreement between simulated sphere packs and macroscopic measures

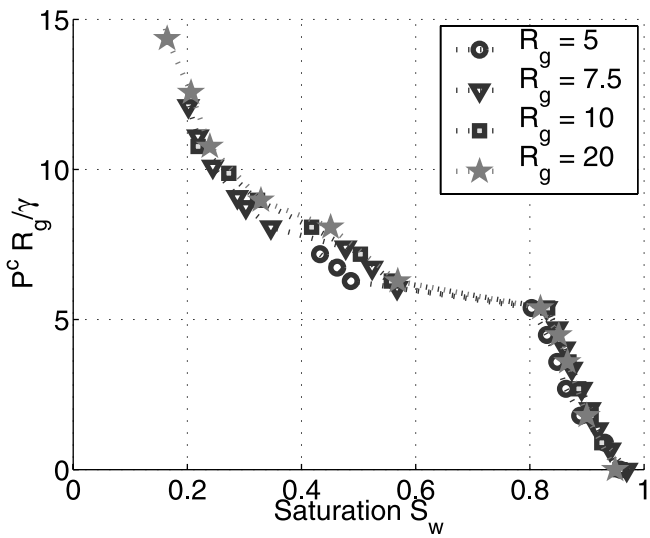

Figure 10. Primary drainage curves for the idealized porous medium shown in Figure 9.

Table 2. Sphere-Packing Realizations for GB1b Porous Medium

Property	Value
Arithmetic mean diameter $\overline{D}$ (mm)	0.1149
Arithmetic standard deviation σ_D (mm)	0.0116
Porosity ϕ	0.356
Domain length L (mm)	2.35
Number of spheres	9,532

typically available for experimental data were achieved here and in other work performed using this approach [*Yang et al.*, 1996; *Pan et al.*, 2001].

[45] Table 2 shows the properties of the simulated packing that represents the experimental GB1b porous medium. The packing contains 9,532 spheres. The output of the sphere-packing code (centers and diameters of the spheres) was then used to generate three-dimensional digital representations of the porous medium. Four levels of discretizations, containing 128^3, 256^3, 384^3, and 512^3 voxels, were generated for the sphere pack used in this work.

[46] The experimentally examined capillary pressure head h^c* (in units of height of water) can be expressed in terms of nondimensional variables:

$$h^{c*} = \frac{P^{c*}}{\rho_w^* g} = \frac{P^c \gamma^*}{\gamma l_0 \rho_w^* g} = \frac{P^c N \gamma^*}{\gamma L \rho_w^* g}. \quad (19)$$

In equation (19), $P^{c*}l_0/\gamma^* = P^c/\gamma$ is used, and so is $l_0 = L/N$, where l_0 is the characteristic length, L is the length of the medium, and N is the discretization level in lattice units. As described previously, the interfacial tension γ* between water and PCE is known to be 36.23 dyn/cm (at 20°C), and the nondimensional interfacial tension $\gamma = 22.71$.

5.2.1. Discretization Effects

[47] We first study how the PD simulation results were affected by the resolution level. Because of computational limitations, we took a 1/64 subdomain of the entire GB1b sphere-pack for this study, which contained approximately 150 spheres; spheres in the system pack were allowed to cross boundaries for any subset of the domain. The lattice sizes used to simulate the subdomain were 32^3, 64^3, 96^3, and 128^3, which correspond to the number of lattice nodes per mean sphere diameter, or ζ, being 6.5, 13.0, 19.5, and 26.0, respectively. The capillary pressure increment was chosen such that there were about 15 points along a PD curve. Figure 11 shows the PD curves for varying levels of discretizations for the 1/64 subdomain of the GB1b sphere pack. The capillary pressure is presented as the height of a corresponding water column h^c*.

[48] The mean pore throat radius in a random packing of uniform spheres is approximated by [*Ng et al.*, 1978]

$$\langle R_t \rangle = 0.21D, \quad (20)$$

from which one can estimate that the NWP entry pressure head is $h^{c*} = 2\gamma^*/(0.21D\rho_w^* g)$. To estimate the entry pressure of the sphere pack representing the GB1b pack using this equation, we assumed D stands for the arithmetic mean grain diameter $\overline{D}$ and then calculated the NWP entry as $h^{c*} = 30.4$ cm. This estimate fall about mid way between the experimental results and the simulated results.

[49] Discretization effects occur because the digital pore space is not self-similar as the resolution changes. It is not surprising that the coarser discretization results in a lower NWP entry pressure, because larger digital pore spaces are more likely to be generated by the coarser discretization than by finer ones. The observation is consistent with our previous investigation, which showed that a coarser discretization yields a larger saturated permeability of a porous medium [*Pan et al.*, 2001]. As shown in the Figure 11, we observed that the simulated PD curve approached convergence if the number of lattice nodes per mean sphere diameter satisfied the inequality $\zeta \geq 13.0$. This result also agrees with our previous investigations [*Pan et al.*, 2001], which found that the saturated permeability becomes essentially discretization-independent if $\zeta > 12$, for packings of both spheres with a uniform size distribution and spheres with a nonuniform size distribution with a relative standard deviation of sphere diameters up to 65%.

[50] We also obtained good agreement between the simulated *P-S* curve and the experimental data. We expected some discrepancy between them because the experiments were performed for the entire medium in a long column [*Hilpert et al.*, 2001], while the LB simulations were based on a cubic subdomain consisting of only about 150 spheres, which we expect to be smaller than the size needed for a representative elementary volume (REV). *Hilpert and Miller* [2001] applied primary drainage simulations using a pore-morphology-based approach on the same GB1b porous medium and suggested that a domain corresponding approximately to 2500 spheres is considered to be a REV.

5.2.2. Hysteretic $P - S$ Curve

[51] Because of computational limitations, we used a 1/64 subset of the entire GB1b sphere pack to simulate main imbibition (MI) and scanning curves originated from the PD curve. The subdomain had about 150 spheres, a nondimensional domain length, $L/\bar{D}$, of 5.1, and 64^3 voxels, resulting in a resolution of $\zeta = 13.0$ and a mean pore throat radius of approximately 2.7 lattice units, estimated using equation (20). In Figure 12 we show the distributions of NWP during primary drainage and main imbibition simulations, in which the capillary pressure head was initialized from zero, first increased incrementally to 78-cm water and then decreased back to 3-cm water.

[52] Figure 13 shows the simulated PD, MI, and imbibition scanning curves for a subdomain with 64^3 voxels. The

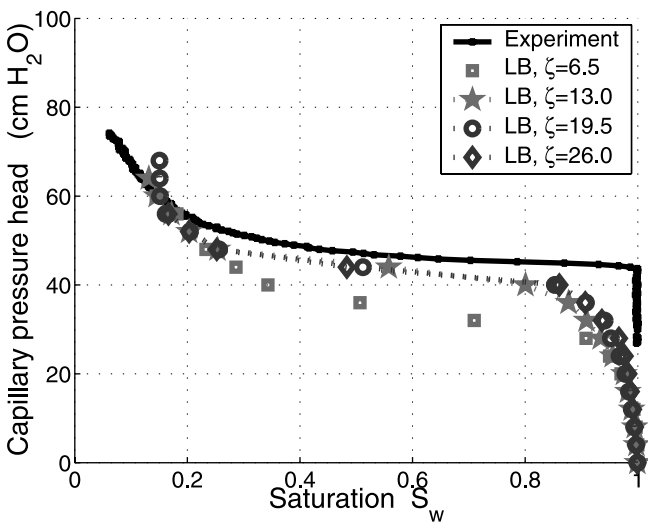

Figure 11. Influence of spatial discretization on primary drainage curve for the GB1b porous medium system.

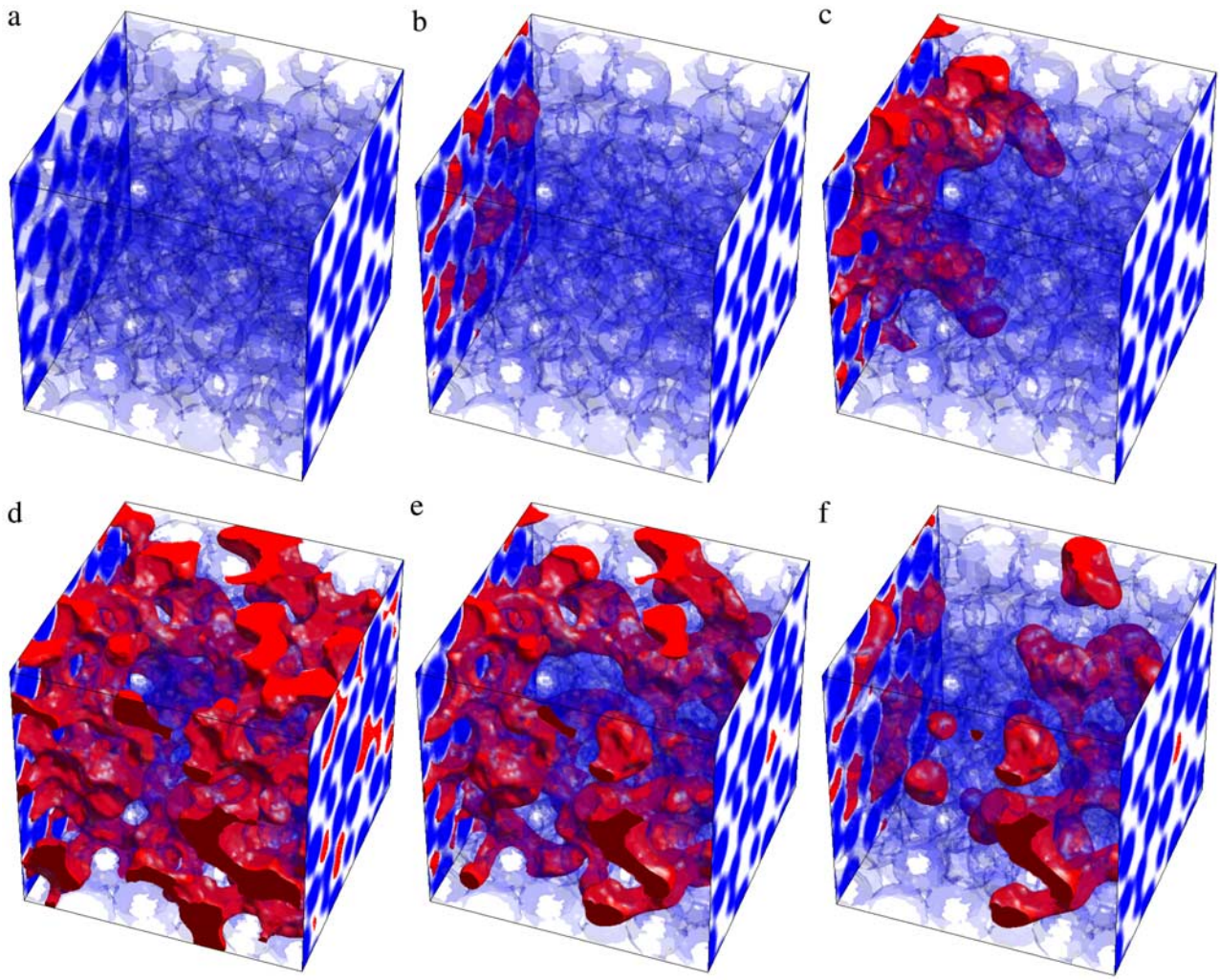

Figure 12. Distributions of nonwetting phase during a primary drainage and main imbibition simulation for the GB1b porous medium system. The transparent blue isosurface indicates the interface between the pore space and the solid phase. Red represents the nonwetting fluid. For clarity of illustration the wetting fluid water is not shown, and the pore space that is not red is considered as being occupied by water. (a) Primary drainage simulation started from $h^c* = 0$, at the equilibrium state $S_w = 1$; (b) $S_w = 0.97$ at $h^c* =$ 26.7 cm H_2O; (c) $S_w = 0.88$ at $h^c* = 40.0$ cm H_2O; (d) $S_w = 0.05$ at $h^c* = 77.3$ cm H_2O; (e) Main

scanning curve was obtained by starting the imbibition process from $h^c* = 46.5$ cm on the drainage curve. Figure 13 shows encouraging agreement between the experimental observations and the LB simulations, including: (1) a good match of the irreducible WP saturation of around 0.04; (2) agreement within about 5% for the NWP residual saturation; (3) capillary pressures for NWP entry that are within a factor of about two; (4) minimum slopes for PD that are within 5%; and (5) the absence of intersection between the main imbibition and the imbibition scanning curves. However, the imbibition scanning curve does not match closely with experimental data. We expected these results because our simulation domain is relatively small, and the sequence of invading pores is critical to simulate imbibition processes.

[53] To investigate the effect of domain size on drainage and imbibition processes, we performed a simulation on a domain containing around 1200 spheres ($L/\overline{D} = 10.2$) with 128^3 voxels ($\zeta = 13.0$). The results are plotted in Figure 13. Compared with the smaller domain, the *P-S* curve simulated for the larger domain shows a slightly lower irreducible saturation, a smaller residual NWP saturation, and a significantly different MI curve, which is closer to the experimental data than the smaller simulated domain. To the best of our knowledge, this is the first time that LB simulations have been performed for such a large system, compared to experimental capillary pressure saturation data, and used to examine the size of REV needed to achieve converged results. Because of the computational limitations, we can only use this to suggest a lower bound on the size of REV. Further work along these lines is clearly needed.

6. Discussion and Summary

[54] We have studied the use of the Shan-Chen lattice Boltzmann approach for modeling immiscible two-fluid-phase flow in porous medium systems, including those

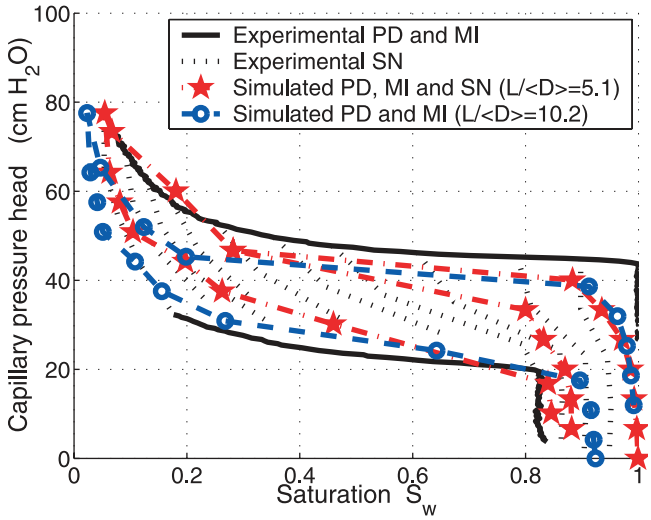

Figure 13. LB simulated primary drainage (PD), main imbibition (MI), and scanning (SN) curve for the GB1b porous medium.

represented by idealized sphere packs intended to mimic an experimental system for which an extensive data set existed. Adjustable parameters in the LB model were determined to match known physical behavior for multiphase systems. The LB model was calibrated to account for different fluid properties, such as densities, viscosities and wetting preferences. By mimicking the experimental two-phase displacement processes, hysteretic *P-S* relations obtained from LB simulations on random packings of spheres show encouraging agreement when compared to experimental data.

[55] The present work is a first step toward enhancing the understanding of multiphase flow mechanisms at the pore scale. We believe that a variety of further investigations on multiphase porous medium flow are possible by using this approach. For example, one can study nonwetting phase trapping as a function of geometry, wettability, viscosity, and capillary number by systematically investigating the pore-scale mechanisms of imbibition, such as snap-off. Other applications include the investigation of the effect of the viscosity ratio on the relative permeabilities and dynamic capillary pressure-fluid saturation relations. We believe that significant fundamental understanding can be achieved through such investigations.

[56] While our simulation results are encouraging, challenges for current two-phase LB flow models remain. First, the applications of the LB model to multiphase flow is limited by the admissible range of fluid properties due to restricted numerical stability. *Chin et al.* [2002] found that using the SC model, numerical instabilities occur when the viscosity ratio between phases becomes larger than 10. Even though the stability issue of the LB methods has not been well understood, this problem has been considered [*Worthing et al.*, 1997; *Lallemand and Luo*, 2000]. It was shown by *Lallemand and Luo* [2000] and *d'Humieres et al.* [2002] that a multiple-relaxation-time (MRT) LB model, which separates relaxations for the kinetic modes, is more stable than the BGK LB model, which uses a single-time relaxation approximation. In addition, a more accurate treatment of boundary conditions at solid-fluid interfaces, which combines the bounce-back scheme and spatial interpolations of first or second order to realize the locations of boundaries with arbitrary curvatures, can be incorporated for further improvement of numerical stability and a more rapid convergence [*Bouzidi et al.*, 2001; *Lallemand and Luo*, 2003]. We believe such studies are important next steps in the evolution of LB modeling of multiphase porous medium systems.

[57] Finally, computational limitations are of great concern when applying LB simulations for multiphase porous medium systems, even using large-scale parallel computing. Our simulator is written in Fortran 90 using the Message Passing Interface (MPI) library. Though the portability of the code has been tested with a variety of compilers on different parallel platforms, the parallel machine we primarily used was an IBM RS/6000 SP with 720 375 MHz Power3-II processors. Our work suggests that simulating primary drainage and imbibition scanning curves (typically 20 points) in a porous medium domain with 64^3 voxels requires more than 4,000 CPU hours and 70 MBs of RAM, while simulating a primary drainage curve (typically 10 points along the curve) in a porous medium domain with 128^3 voxels requires around 50,000 CPU hours. As a result, we cannot currently afford to simulate larger domains, which would yield results closer to an REV. Because the lattice is uniform, many lattice points fall within the solid phase, and thus do not possess active distributions of fluid probabilities. In order to reduce computational time and memory requirements, we have recently developed a new and efficient parallel code that disregards the solid lattice points [*Pan*, 2003].

[58] **Acknowledgments.** This work was supported by National Science Foundation grant EAR-9901660, National Institute of Environmental Health Science grant P42 ES05948, and a generous allocation of computing time from the North Carolina Supercomputing Center. Partial support of this work was also provided by the National Science Foundation through DMS-0112069 to the Statistical and Applied Mathematical Sciences Institute in Research Triangle Park, where a portion of this work was done.

References

Abriola, L. M. (1988), Multiphase flow and transport models for organic chemicals: A review and assessment, *Tech. Rep. EPRI EA-5976*, Electric Power Res. Inst., Palo Alto, Calif.

Abriola, L. M., and G. F. Pinder (1985), A multiphase approach to the modeling of porous media contamination by organic compounds: 1. Equation development, *Water Resour. Res.*, *21*(1), 11–18.

Adler, P. M. (1992), *Porous Media: Geometry and Transports*, Butterworth-Heinemann, Woburn, Mass.

Aziz, K., and A. Settari (1979), *Petroleum Reservoir Simulation*, Appl. Sci., London.

Baldwin, C. A., A. J. Sederman, M. D. Mantle, P. Alexander, and L. F. Gladden (1996), Determination and characterization of the structure of a pore space from 3d volume images, *J. Colloid Interface Sci.*, *181*, 79.

Bear, J. (1972), *Dynamics of Fluids in Porous Media*, Elsevier Sci., New York.

Bekri, S., and P. M. Adler (2002), Dispersion in multiphase flow through porous media, *Int. J. Multiphase Flow*, *28*(4), 665–697.

Bekri, S., J. Howard, J. Muller, and P. M. Adler (2003), Electrical resistivity index in multiphase flow through porous media, *Transp. Porous Media*, *51*(1), 41–65.

Bhatnagar, P., E. Gross, and M. Krook (1954), A model for collsion processes in gases, *Phys. Rev.*, *94*, 511–525.

Blunt, M. (2001), Flow in porous media—Pore-network models and multiphase flow, *Curr. Opinion Colloid Interface Sci.*, *6*(3), 197–207.

Blunt, M., and P. King (1991), Relative permeabilities from two- and three-dimensional pore scale network modeling, *Transp. Porous Media*, *6*(4), 407–434.

Boghosian, B. M., and P. V. Coveney (2000), A particulate basis for an immiscible lattice-gas model, *Comput. Phys. Commun.*, *129*(1–3), 46–55.

Bosl, W. J., J. Dvorkin, and A. Nur (1998), A study of porosity and permeability using a lattice Boltzmann simulation, *Geophys. Res. Lett.*, *25*(9), 1475–1478.

Bouzidi, M., M. Firdaouss, and P. Lallemand (2001), Momentum transfer of a Boltzmann-lattice fluid with boundaries, *Phys. Fluids*, *13*(11), 3452–3459.

Buckles, J. J., R. D. Hazlett, S. Chen, K. G. Eggert, D. W. Grunau, and W. E. Soll (1994), Toward improved prediction of reservoir flow performance: Simulating oil and water flows at the pore scale, *Los Alamos Science*, *22*, 113–121.

Celia, M. A., P. C. Reeves, and L. C. Ferrand (1995), Recent advances in pore scale models for multiphase flow in porous media, *Rev. Geophys.*, *33*, 1049–1057.

Chen, H., S. Chen, and W. H. Matthaeus (1992), Recovery of the Navier-Stokes equations using a lattice-gas Boltzmann methods, *Phys. Rev. A*, *45*, 5339–5342.

Chen, S., and G. D. Doolen (1998), Lattice Boltzmann method for fluid flows, *Annu. Rev. Fluid Mech.*, *30*, 329–364.

Chin, J., E. S. Boek, and P. V. Coveney (2002), Lattice Boltzmann simulation of the flow of binary immiscible fluids with different viscosities using the Shan-Chen microscopic interaction model, *Philos. Trans. R. Soc. London, Ser. A*, *360*, 547–558.

Cushman, J. H. (1990), *Dynamics of Fluids in Hierarchical Porous Media*, Academic, San Diego, Calif.

Desplat, J. C., I. Pagonabarraga, and P. Bladon (2001), Ludwig: A parallel lattice-Boltzmann code for complex fluids, *Comput. Phys. Commun.*, *134*, 273–290.

d'Humieres, D., I. Ginzburg, M. Krafczyk, P. Lallemand, and L. S. Luo (2002), Multiple-relaxation-time lattice Boltzmann models in three dimensions, *Philos. Trans. R. Soc. London, Ser. A*, *360*, 437–451.

Dias, M. M., and A. C. Payatakes (1986), Network models for two-phase flow in porous media, part 1, Immiscible microdisplacement of non-wetting fluids, *J. Fluid Mech.*, *164*, 305–336.

Dillard, L. A., and M. J. Blunt (2000), Development of a pore network simulation model to study nonaqueous phase liquid dissolution, *Water Resour. Res.*, *36*(2), 439–454.

Fan, L., H. Fang, and Z. Lin (2001), Simulation of contact line dynamics in a two-dimensional capillary tube by the lattice Boltzmann model, *Phys. Rev. E.*, *63*, 051603, 1–6.

Ferréol, B., and D. H. Rothman (1995), Lattice-Boltzmann simulations of flow through Fontainebleau sandstone, *Transp. Porous Media*, *20*, 3–20.

Grunau, D., S. Chen, and K. Eggert (1993), A lattice Boltzmann model for multiphase fluid flows, *Phys. Fluids A*, *5*(10), 2557–2562.

Gunstensen, A. K., D. H. Rothman, S. Zaleski, and G. Zanetti (1991), Lattice Boltzmann model of immiscible fluids, *Phys. Rev. A*, *43*(8), 4320–4327.

Hazi, G., A. R. Imre, G. Mayer, and I. Farkas (2002), Lattice Boltzmann methods for two-phase flow modeling, *Ann. Nucl. Energy*, *29*, 1421–1453.

Hazlett, R. D., and R. N. Vaidya (2002), Lattice Boltzmann simulations and contact angle hysteresis in convergent-divergent media, *J. Pet. Sci. Eng.*, *33*, 161–171.

He, X., and G. D. Doolen (2002), Thermodynamics foundations of kinetic theory and lattice Boltzmann models for multiphase flows, *J. Stat. Phys.*, *107*(1/2), 309–328.

He, X., X. Shan, and G. D. Doolen (1998), Discrete Boltzmann equation model for nonideal gas, *Phys. Rev. E*, *57*(1), R13–R16.

He, X. Y., S. Y. Chen, and R. Y. Zhang (1999), A lattice Boltzmann scheme for incompressible multiphase flow and its application in simulation of Rayleigh-Taylor instability, *J. Comput. Phys.*, *152*(2), 642–663.

Hilpert, M., and C. T. Miller (2001), Pore-morphology-based simulation of drainage in totally wetting porous media, *Adv. Water Resour.*, *24*(3/4), 243–255.

Hilpert, M., J. F. McBride, and C. T. Miller (2001), Investigation of the residual-funicular nonwetting-phase-saturation relation, *Adv. Water Resour.*, *24*(2), 157–177.

Hilpert, M., R. Glantz, and C. T. Miller (2003), Calibration of a pore-network model by a pore-morphological analysis, *Transp. Porous Media*, *51*(3), 267–285.

Holdych, D. J., D. Roves, J. G. Geogiadis, and R. O. Buckius (1998), An improved hydrodynamics formulation for multiphase flow lattice Boltzmann methods, *Int. J. Modern Phys. C*, *9*, 1393–1404.

Hou, S., Q. Zou, S. Chen, G. Doolen, and A. C. Cogley (1995), Simulation of cavity flow by the lattice Boltzmann method, *J. Comput. Phys.*, *118*, 329–347.

Hou, S. L., X. W. Shan, Q. S. Zuo, G. D. Doolen, and W. E. Soll (1997), Evaluation of two lattice Boltzmann models for multiphase flows, *J. Comput. Phys.*, *138*(2), 695–713.

Ihle, T., and D. M. Kroll (2000), Thermal lattice-Boltzmann method for non-ideal gases with potential energy, *Comput. Phys. Commun.*, *129*(1–3), 1–12.

Kalarakis, A. N., V. N. Burganos, and A. C. Payatakes (2002), Galilean-invariant lattice-Boltzmann simulation of liquid-vapor interface dynamics, *Phys. Rev. E*, *65*, 056702.

Kalarakis, A. N., V. N. Burganos, and A. C. Payatakes (2003), Three-dimensional lattice-Boltzmann model of van del Waals fluids, *Phys. Rev. E*, *67*, 016702.

Kandhai, D., A. Koponen, A. G. Hoekstra, M. Katajam, J. Timonen, and P. M. A. Sloot (1998), Lattice-Boltzmann hydrodynamics on parallel systems, *Comput. Phys. Commun.*, *111*, 14–26.

Kang, Q. J., D. X. Zhang, and S. Y. Chen (2002), Displacement of a two-dimensional immiscible droplet in a channel, *Phys. Fluids*, *14*(9), 3203–3214.

Koplik, J. and T. J. Lasseter (1982), Two-phase flow in random network models of porous media, paper presented at 57th Annual Fall Technical Conference and Exhibition of the Society of Petroleum Engineers of AIME, Am. Inst. of Min., Metall., and Pet. Eng., New Orleans, La.

Lallemand, P., and L. S. Luo (2000), Theory of the lattice Boltzmann method: Dispersion, dissipation, isotropy, Galilean invariance, and stability, *Phys. Rev. E*, *61*(6), 6546–6562.

Lallemand, P., and L. S. Luo (2003), Lattice Boltzmann method for moving boundaries, *J. Comput. Phys.*, *184*, 406–421.

Lenormand, R., and C. Zarcone (1988), Physics of blob displacement in a two-dimensional porous medium, *SPE Form. Eval.*, *3*, 271–275.

Lin, C., and M. H. Cohen (1982), Quantitative methods for microgeometric modeling, *J. Appl. Phys.*, *53*(6), 4152–4165.

Lowry, M. I., and C. T. Miller (1995), Pore-scale modeling of nonwetting-phase residual in porous media, *Water Resour. Res.*, *31*(3), 455–473.

Luo, L. S. (1998), Unified theory of lattice Boltzmann models for nonideal gases, *Phys. Rev. Lett.*, *81*(8), 1618–1621.

Luo, L. S., and S. S. Girimaji (2003), Theory of the lattice Boltzmann method: Two-fluid model for binary mixtures, *Phys. Rev. E*, *67*, 036302.

Maier, R. S., D. M. Kroll, Y. E. Kutsovsky, H. T. Davis, and R. S. Bernard (1998), Simulation of flow through bead packs using the lattice Boltzmann method, *Phys. Fluids*, *10*(1), 60–74.

Man, H. N., and X. D. Jing (2000), Pore network modelling of electrical resistivity and capillary pressure characteristics, *Transp. Porous Media*, *41*(3), 263–286.

Mantle, M. D., A. J. Sederman, and L. F. Gladden (2001), Single-and two-phase flow in fixed-bed reactors: MRI flow visualization and lattice-Boltzmann simulations, *Chem. Eng. Sci.*, *56*, 523–529.

Martys, N., and H. Chen (1996), Simulation of multicomponent fluids in complex three-dimensional geometries by the lattice Boltzmann method, *Phys. Rev. E*, *53*(1b), 743–750.

Martys, N. S., and J. F. Douglas (2001), Critical properties and phase separation in lattice Boltzmann fluid mixtures, *Phys. Rev. E*, *63*(3), 031205.

Martys, N. S., S. Torquato, and D. P. Bentz (1994), Universal scaling of fluid permeability for sphere packings, *Phys. Rev. E*, *50*(1), 403–408.

Mayer, A. S. and C. T. Miller (1990), A compositional model for simulating multiphase flow, transport and mass transfer in groundwater systems, in *Proceedings of the Eighth International Conference on Computational Methods in Water Resources, Computational Methods in Subsurface Hydrology*, edited by G. Gambolati, et al., pp. 217–222, Springer-Verlag, New York.

Mayer, A. S., and C. T. Miller (1992), The influence of porous medium characteristics and measurement scale on pore-scale distributions of residual nonaqueous-phase liquids, *J. Contam. Hydrol.*, *11*(3/4), 189–213.

Miller, C. T., and W. G. Gray (2002), Hydrogeological research: Just getting started, *Ground Water*, *40*(3), 22400231.

Miller, C. T., G. Christakos, P. T. Imhoff, J. F. McBride, J. A. Pedit, and J. A. Trangenstein (1998), Multiphase flow and transport modeling in heterogeneous porous media: Challenges and approaches, *Adv. Water Resour.*, *21*(2), 77–120.

Ng, K. M., H. T. Davis, and L. E. Scriven (1978), Visualization of blob mechanics in flow through porous media, *Chem. Eng. Sci.*, *33*, 1009–1017.

Nourgaliev, R. R., T. N. Dinh, T. G. Theofanous, and D. Joseph (2003), The lattice Boltzmann equation method: Theoretical interpretation, numerics and implications, *Int. J. Multiphase Flow*, *29*, 117–169.

Oren, P. E., and W. V. Pinczewski (1995), Fluid distribution and pore-scale displacement mechanisms in drainage dominated three-phase flow, *Transp. Porous Media*, *20*(1–2), 105–133.

Pan, C. (2003), Use of pore-scale modeling to understand flow and transport in porous media, Ph.D. thesis, Univ. of N. C., Chapel Hill.

Pan, C., M. Hilpert, and C. T. Miller (2001), Lattice-Boltzmann simulation of multiphase flow in water-wet porous media, *Eos Tran. AGU*, *82*(47), Fall Meet. Suppl., Abstract H21F-05.

Paunov, V. N., A. Angelopoulos, and V. N. Burganos (1996), Lattice-Boltzmann simulation of ideal and nonideal immiscible two-phase flow in porous media, in *Computational Methods in Water Resources XI*, vol. 1, *Computational Methods in Subsurface Flow and Transport Problems*, edited by A. A. Aldama et al., pp. 457–464, Comput. Mech., Southampton, U. K.

Pereira, G. G. (1999), Numerical pore-scale modeling of three-phase fluid flow: Comparison between simulation and experiment, *Phys. Rev. E*, *59*(4), 4229–4242.

Rothman, D. H., and J. M. Keller (1988), Immiscible cellular-automaton fluids, *J. Stat. Phys.*, *52*(3/4), 1119–1127.

Rothman, D. H., and S. Zaleski (1997), *Lattice-Gas Cellular Automata: Simple Models of Complex Hydrodynamics*, Cambridge Univ. Press, New York.

Schiegg, H. O. (1979), Verdrängungs-Simulation dreier nicht mischbarer Fluide in poröser Matrix, Mitt. Versuchsanstalt Wasserbau, Hydrol. Glaziol. 40, Eidg. Tech. Hochsch. Zürich, Zurich, Switzerland.

Schiegg, H. O. (1990), Laboratory setup and results of experiments on two-dimensional multiphase flow in porous media, *Tech. Rep. PNL-7453*, Pac. Northwest Lab., Richland, Wash.

Sederman, A. J., M. L. Johns, A. S. Bramlet, P. Alexander, and L. F. Gladden (1997), Magnetic resonance imaging of liquid flow and pore stricture-flow correlations in packed beds, *Chem. Eng. Sci.*, *52*, 2239–2250.

Shan, X., and H. Chen (1993), Lattice Boltzmann model for simulating flows with multiple phases and components, *Phys. Rev. E*, *47*, 1815–1819.

Shan, X., and H. Chen (1994), Simulation of nonideal gases and liquid-gas phase transitions by the lattice Boltzmann equation, *Phys. Rev. E*, *49*(4), 2941–2948.

Shan, X., and G. Doolen (1995), Multicomponent lattice-Boltzmann model with interparticle interaction, *J. Stat. Phys.*, *81*(1/2), 379–393.

Shan, X., and G. Doolen (1996), Diffusion in a multi-conponent lattice Boltzmann equation model, *Phys. Rev. E*, *54*(4), 3614–3620.

Soll, W. E., S. Y. Chen, K. G. Eggert, D. W. Grunau, and D. R. Janecky (1994), Application of the lattice Boltzmann/lattice gas technique to multi-fluid flow in porous media, in *Computational Methods in Water Resources X*, vol. 2, edited by A. Peters, et al., pp. 991–1000, Kluwer Acad., Norwell, Mass.

Spanne, P., J. F. Thovert, C. J. Jacquin, W. B. Lindquist, K. W. Jones, and P. M. Adler (1994), Synchrotron computed microtomography of porous media, *Phys. Rev. Lett.*, *73*, 2001–2004.

Succi, S., E. Foti, and F. Higuera (1989), Three dimensional flows in complex geometries with the lattice Boltzmann methods, *Europhys. Lett.*, *10, 433.*

Swift, M. R., W. R. Osborn, and J. M. Yeomans (1995), Lattice Boltzmann simulation of nonideal fluids, *Phys. Rev. Lett.*, *75*(5), 830–833.

Swift, M. R., E. Orlandini, W. R. Osborn, and J. M. Yeomans (1996), Lattice Boltzmann simulations of liquid-gas and binary fluid systems, *Phys. Rev. E*, *54*(5), 5041–5052.

Thompson, K. E. (2002), Pore-scale modeling of fluid transport in disordered fibrous materials, *AIChE J.*, *48*(7), 1369–1389.

Tolke, J., X. Krafczyk, M. Schulz, and E. Rank (2002), Lattice Boltzmann simulations of binary fluid flow through porous media, *Philos. Trans. R. Soc. London, Ser. A*, *360*, 535–545.

van Genabeek, O., and D. H. Rothman (1996), Macroscopic manifestations of microscopic flows through porous media, Phenomenology from simulation, *Annu. Rev. Earth Planet. Sci.*, *24*, 63–87.

Worthing, R. A., J. Mozer, and G. Seeley (1997), Stability of lattice Boltzmann methods in hydrodynamic regimes, *Phys. Rev. E*, *56*(2), 2243–2253.

Yang, A., C. T. Miller, and L. D. Turcoliver (1996), Simulation of correlated and uncorrelated packing of random size spheres, *Phys. Rev. E*, *53*(2), 1516–1524.

Yang, Z. L., T. N. Dinh, R. R. Nourgaliev, and B. R. Sehgal (2000), Evaluation of the Darcy's law performance for two-fluid flow hydrodynamics in a particle debris bed using a lattice-Boltzmann model, *Heat Mass Transfer*, *36*(4), 295–304.

Yao, J., P. Frykman, F. Kalaydjian, J. F. Thovert, and P. M. Adler (1993), High-order moments of the phase function for real and reconstructed model porous-media—A comparison, *J. Colloid Interface Sci.*, *156*(2), 478–490.

Zhang, D., R. Zhang, S. Chen, and W. E. Soll (2000), Pore scale study of flow in porous media: Scale dependency, REV, and statistical REV, *Geophys. Res. Lett.*, *27*(8), 1915–1918.

Zhang, R., X. He, and S. Chen (2000), Interface and surface tension in incompressible lattice Boltzmann multiphase model, *Comput. Phys. Commun.*, *129*(121–130).

M. Hilpert, Department of Geography and Environmental Engineering, Johns Hopkins University, 313 Ames Hall, 3400 North Charles Street, Baltimore, MD 21218-2686, USA. (markus_hilpert@jhu.edu)

C. T. Miller and C. Pan, Department of Environmental Sciences and Engineering, University of North Carolina, Chapel Hill, NC 27599-7431, USA. (casey_miller@unc.edu; dpan@email.unc.edu)